

Redox-Inactive Metal Cations Modulate the Reduction Potential of the Uranyl Ion in Macrocyclic Complexes

Amit Kumar,[#] Davide Lionetti,^{#,†} Victor W. Day,[#] and James D. Blakemore^{*,*}

[#]Department of Chemistry, University of Kansas, 1567 Irving Hill Road, Lawrence, Kansas 66045, United States

Supporting Information Placeholder

ABSTRACT: Capture and activation of the water-soluble uranyl dication (UO_2^{2+}) remains a challenging problem, as few rational approaches are available for modulating the reactivity of this species. Here, we report the divergent synthesis of heterobimetallic complexes in which UO_2^{2+} is held in close proximity to a range of redox-inactive metals by a tailored macrocyclic ligand. Crystallographic and spectroscopic studies confirm assembly of homologous $\text{U}^{\text{VI}}(\mu\text{-O}_M)_2\text{M}^{\text{n+}}$ cores with a range of mono-, di-, and tri-valent Lewis acids ($\text{M}^{\text{n+}}$). Cyclic voltammetry data demonstrate that the $\text{U}^{\text{VI}}/\text{U}^{\text{V}}$ reduction potential in these complexes is modulated over a span of 600 mV, depending linearly on the Lewis acidity of the redox-inactive metal with a sensitivity of $61 \pm 9 \text{ mV/p}K_a$ unit. These findings suggest that interactions with Lewis acids could be effectively leveraged for rational tuning of the electronic and thermochemical properties of the $5f$ elements, reminiscent of strategies more commonly employed with $3d$ transition metals.

1. INTRODUCTION

Nuclear fission of uranium is attractive for meeting current and future energy needs, in that this technology does not release significant amounts of carbon dioxide during routine use. However, separation and reprocessing of used nuclear fuels, aspects that are critical to the long-term viability of this technology, remain challenging due in part to difficulties associated with chemical transformation of various forms of uranium. Specifically, (re)processing of uranium requires cleavage of strong and chemically robust U–O bonds.^{1,2,3} The U–O bonds in the water-soluble uranyl dication (UO_2^{2+}) are known to be especially strong ($\Delta H_{\text{U-O,gas}} = 148 \text{ kcal mol}^{-1}$), contributing to this species' persistence in the environment and its importance in model studies of U–O bond activation.⁴

In the field of UO_2^{2+} chemistry,⁵ scattered reports suggest that Lewis acids can become involved in U–O activation. Arnold, Love, and co-workers, in the context of studying silylation of UO_2^{2+} by trimethylsilylamide in the presence of a strong reductant,⁶ found that the desired U^{V} products were stabilized by a Lewis acid (Fe^{2+} or Zn^{2+}) present in a nearby binding site. Notably, U^{V} complexes could not be isolated without the addition of Fe^{2+} or Zn^{2+} , suggesting a key role for these metal cations. Complementary work from Hayton and co-workers and Arnold, Love, and co-workers have shown significant positive shifts in $E(\text{U}^{\text{VI}}/\text{U}^{\text{V}})$ caused by functionalization of the oxo moieties with Lewis acidic electrophilic groups (e.g., SiR_3 , $\text{B}(\text{C}_6\text{F}_5)_3$).^{7,8,9,10} Mazzanti and co-workers have also measured a positive shift in $E(\text{U}^{\text{VI}}/\text{U}^{\text{V}})$ upon association of UO_2^{2+} complexes with Fe^{2+} .¹¹ However, no quantitative studies

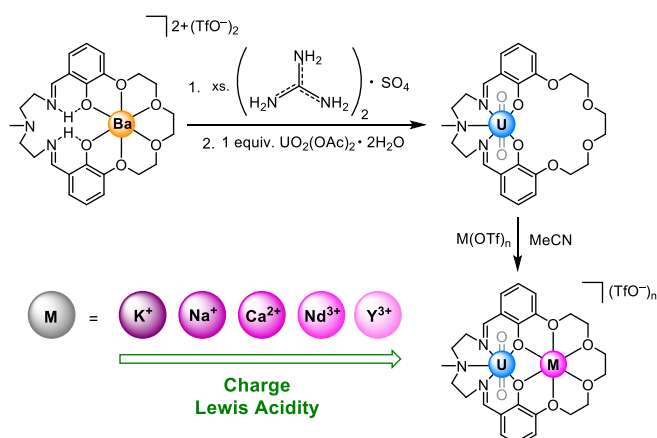
of reduction potential tuning of $E(\text{U}^{\text{VI}}/\text{U}^{\text{V}})$ for UO_2^{2+} or other redox processes in $5f$ species by Lewis acidic metal cations are available.

From the field of first-row transition metal chemistry, an effective strategy for rationally tuning the properties and reactivity of redox-active complexes involves placement of redox-inactive Lewis acidic metal cations in close proximity to the redox-active metals. This approach is inspired by the presence of an essential redox-inactive Ca^{2+} ion in the Oxygen-Evolving Complex (OEC) of Photosystem II, the enzyme responsible for biological O_2 evolution.^{12,13} Agapie and co-workers' studies of related multimetallic clusters incorporating redox-inactive metals have revealed that the cluster reduction potentials vary linearly with the Lewis acidity of the incorporated redox-inactive ions across a broad range.^{14,15} Thus, the requirement for the Ca^{2+} ion can at least in part be ascribed to tuning of the reduction potential(s) of the nearby redox-active manganese ions present in the OEC.

Related tuning effects have been obtained in artificial transition metal catalysts by the interaction of metal oxo moieties with Lewis acidic metal cations (e.g., Sc^{3+}).^{16,17} These effects are broadly useful as shown by Nam and Fukuzumi^{18,19} as well as Borovik.^{20,21} Alternatively, heteroditopic ligand frameworks with well-defined sites for binding of both redox-active and redox-inactive metals can be used to study heterometallic effects.²² Yang has used a convergent synthetic approach with such a strategy to assemble Co and Fe compounds.^{23,24} This approach is reminiscent of work from Matsunaga and Shibasaki, in which they prepared diverse families of dinuclear Schiff base compounds for use as catalysts.²⁵ On the other hand, our group has used a divergent approach with a related scaffold to afford rapid access to various heterobimetallic complexes of Ni, including species featuring important trivalent Lewis acids.²⁶ Considering the lack of quantitative data on redox tuning of UO_2^{2+} by redox-inactive Lewis acids, we anticipated that the modularity of our synthetic approach might enable preparation of new UO_2^{2+} complexes with a range of Lewis acids for new studies of redox tuning.

Here, we report the divergent synthesis and study of macrocyclic heterobimetallic complexes of UO_2^{2+} with a range of redox-inactive Lewis acidic metal cations (namely, K^+ , Na^+ , Ca^{2+} , Nd^{3+} , and Y^{3+}). These redox-inactive metals span a wide range of Lewis acidity, as judged by the $\text{p}K_a$ values of their corresponding metal aqua cations ($\text{p}K_a = 16.0$ for K^+ , 8.3 for Y^{3+}).²⁷ Notably, the synthesized compounds (Scheme 1) are the first examples of structurally characterized heterobimetallic macrocyclic UO_2^{2+} complexes, and thus they complement analogous structures that feature bridging ligands but lack a stabilizing macrocyclic environment.^{28,29,30} Spectroscopic and structural characterization in concert with electrochemical studies reveal that the compounds are

stable in solution and that, as a result, the U^{VI}/U^V reduction potential can be rationally tuned in the complexes. This tuning effect is engendered by the proximity of the UO_2^{2+} ion to the Lewis acids within the macrocyclic frameworks.



Scheme 1. Synthesis of heterobimetallic complexes of UO_2^{2+} .

2. RESULTS

2.1 Synthesis and characterization of the heterobimetallic species

Our heterobimetallic complexes are based upon a family of ditopic macrocycles developed by Reinhoudt^{31,32} and elaborated upon by Vignato^{33,34,35,36} that feature a Schiff-base binding site for UO_2^{2+} that is appended with a second crown-ether-like site for binding of redox-inactive metal cations. Our synthetic strategy (Scheme 1) centers on preparation of a common uranyl-containing macrocyclic compound $L^{salben}UO_2$ that can undergo divergent metalation with suitable reagents to install the redox-inactive metal cations. $L^{salben}UO_2$ was prepared from $L^{salben}H_2Ba$, a previously known compound lacking prior structural characterization.³⁵ Single crystals of $L^{salben}H_2Ba$ suitable for X-ray diffraction (XRD) analysis were grown, confirming the presence of a pentadentate pocket (featuring one trialkylamine, two imine moieties, and two phenol groups) that is poised to bind UO_2^{2+} (Figure 1).

Indeed, the UO_2^{2+} complex $L^{salben}UO_2$ can be synthesized by stirring 1 equiv. of $L^{salben}H_2Ba$ with 10 equiv. of guanidinium sulfate in a biphasic water/chloroform system. Subsequent treatment of the organic layer with $UO_2(OAc)_2 \cdot 2H_2O$ affords $L^{salben}UO_2$ as a red solid.³⁵ As predicted from nuclear magnetic resonance (NMR) experiments (see SI, Figure S5), single-crystal XRD analysis confirms the coordination of UO_2^{2+} in $L^{salben}UO_2$ to the pentadentate Schiff-base cavity of L^{salben} (Figure 1). The pentadentate site provides the desired L_3X_2 -type coordination environment, with the result that no further ligands are bound to the formally U^{VI} center beyond the two oxo groups and the macrocycle. This situation leaves the adjacent crown ether-like cavity open and poised to bind Lewis acidic metals.

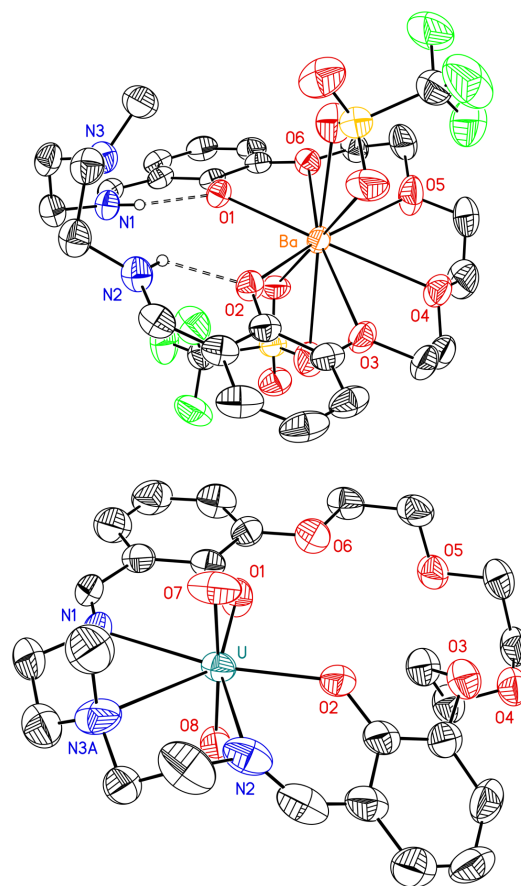


Figure 1. Solid-state structure (from XRD) of $L^{salben}H_2Ba$ (above) and $L^{salben}UO_2$ (below). Outer-sphere triflate counteranions and H-atoms are omitted for clarity. Displacement ellipsoids are shown at the 50% probability level.

The heterobimetallic complexes of the form $L^{salben}UO_2M$ can be prepared by reaction of $L^{salben}UO_2$ with the corresponding metal triflate salts.²⁶ Specifically, treatment of $L^{salben}UO_2$ with triflate salts of K^+ , Na^+ , Ca^{2+} , Nd^{3+} , and Y^{3+} results in the generation of 1:1 heterobimetallic compounds with virtually quantitative yield in each case. 1H NMR spectra (see SI, Figures S6, S8, S10, S12 and S14) indicate that the redox-inactive metal ions are bound in the crown ether-like site of $L^{salben}UO_2$ and that the complexes are stable in CH_3CN solution (see Experimental Section for detailed synthetic procedures and full characterization). Notably, no evidence of scrambling of the metal ions between the two binding sites was observed, confirming the utility of the L^{salben} scaffold in divergent synthetic schemes relying on orthogonal metalation.

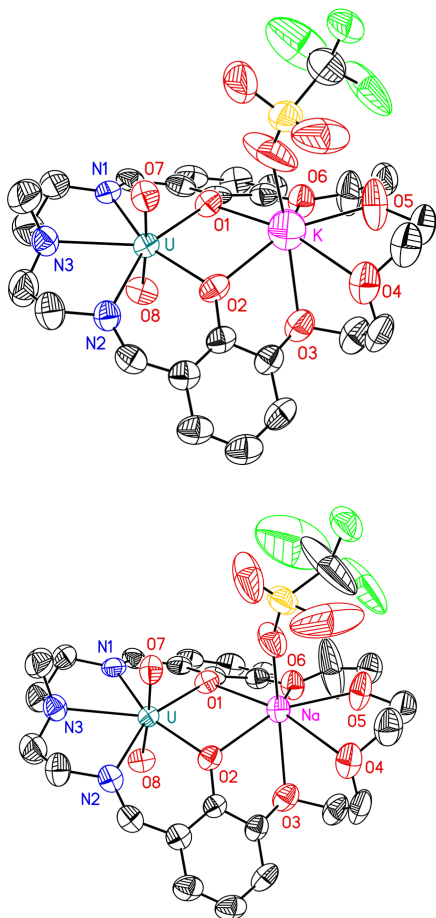


Figure 2. Solid-state structure (from XRD) of $L^{\text{salben}}\text{UO}_2\text{K}$ (above) and $L^{\text{salben}}\text{UO}_2\text{Na}$ (below). Outer-sphere triflate counteranions and all H-atoms are omitted for clarity. Displacement ellipsoids are shown at the 50% probability level.

2.2 X-ray diffraction studies

XRD analysis of single crystals of the heterobimetallic complexes containing K^+ , Na^+ , Ca^{2+} , and Y^{3+} confirms assembly of the desired $\text{U}^{\text{VI}}(\mu\text{-O}_{\text{Ar}})_2\text{M}^{\text{III}}$ cores. The UO_2^{2+} moiety remains structurally intact in all the compounds, with $\text{U}-\text{O}_{\text{oxo}}$ distances in a tight range from 1.771(6) to 1.795(4) Å (see Table 1 for structural parameters). $L^{\text{salben}}\text{UO}_2\text{Na}$ and $L^{\text{salben}}\text{UO}_2\text{K}$ crystallize with isomorphous structures, confirming incorporation of the redox-inactive ions in the crown-ether cavity with coordination numbers (CN) of seven (Figure 2). XRD analysis of $L^{\text{salben}}\text{UO}_2\text{Ca}$ and $L^{\text{salben}}\text{UO}_2\text{Y}$ reveals a higher CN of nine for the redox-inactive ions in these compounds, consistent with the larger size of Ca^{2+} and Y^{3+} (Figure 3). In $L^{\text{salben}}\text{UO}_2\text{Ca}$, the Ca^{2+} ion is ligated by six macrocyclic O-atoms, two MeOH ligands, and one κ^1 triflate. In $L^{\text{salben}}\text{UO}_2\text{Y}$, Y^{3+} is ligated by six macrocyclic O-atoms, one bound CH_3CN ligand, and two κ^1 triflates. Thus, for both $L^{\text{salben}}\text{UO}_2\text{Ca}$ and $L^{\text{salben}}\text{UO}_2\text{Y}$, one triflate counter-anion is outer-sphere. This finding contrasts with our prior work on analogous $[\text{Ni},\text{Ca}]$ and $[\text{Ni},\text{Y}]$ complexes, in which two and three triflate counter-anions, respectively, are coordinated to the redox-inactive metal rather than being found in the outer sphere.²⁶

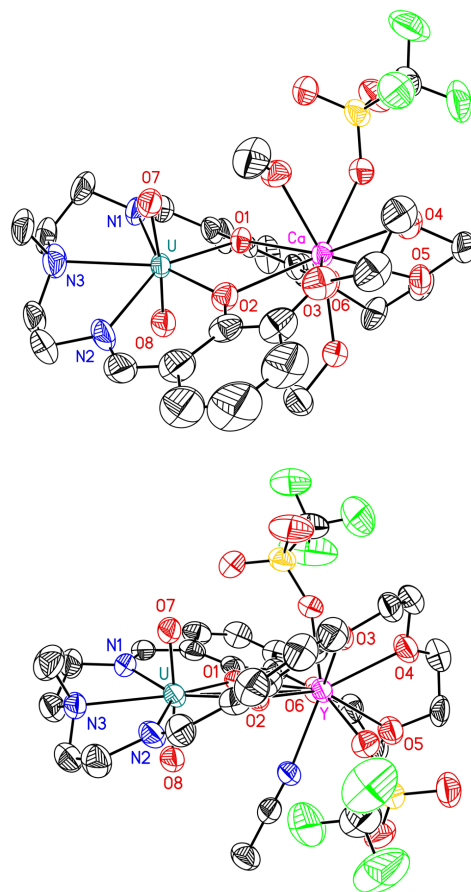


Figure 3. Solid-state structure (from XRD) of $L^{\text{salben}}\text{UO}_2\text{Ca}$ (above) and $L^{\text{salben}}\text{UO}_2\text{Y}$ (below). Outer-sphere triflate counteranions and all H-atoms are omitted for clarity. Displacement ellipsoids are shown at the 50% probability level.

The XRD data reveal that the macrocyclic structure is significantly deformed upon coordination of the Lewis acidic metals. Deformation of the crown-ether-like site across the family of compounds was quantified by comparing the root mean square deviation of the six macrocyclic O-atoms from the mean plane defined from the positions of those atoms (defined as ω_{crown} ; see SI and Table 1 for details). For the heterobimetallic compounds, ω_{crown} varies from 0.609 to 0.717 Å, a significant increase from the value of 0.358 measured for $L^{\text{salben}}\text{UO}_2$. In part, the distortion in the bimetallic compounds may be ascribable to steric clash induced by the spatially demanding pentadentate site containing the UO_2^{2+} moiety; this situation is reflected in low values for the related $\omega_{\text{salben_parameter}}$ in all the uranyl-containing compounds. Consistent with this model, the ω_{crown} value for $L^{\text{salben}}\text{H}_2\text{Ba}$ (0.233) is significantly lower than that for $L^{\text{salben}}\text{UO}_2$ (Figure 1). Furthermore, the $\text{O}1\cdots\text{O}2$ distance is significantly compressed as the Lewis acidity of M increases, corresponding to a drawing together of these macrocyclic atoms upon coordination of the redox-inactive metals.

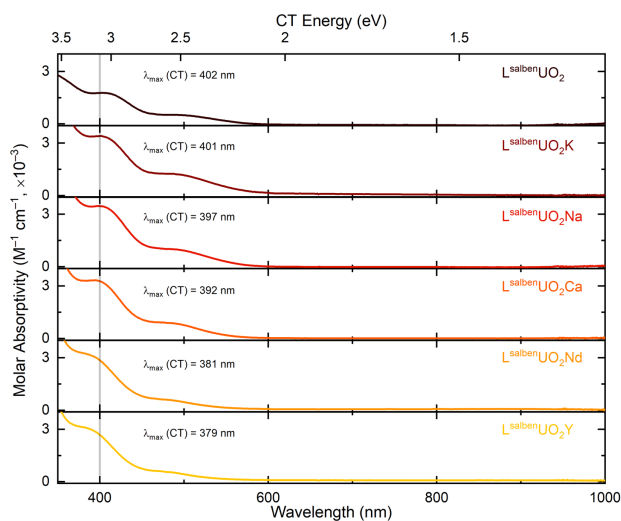
Table 1. Comparison of $[M(H_2O)_m]^{n+}$ complex pK_a values, selected bond lengths, interatomic distances, and root mean square deviations (ω).

	$L^{salben}H_2Ba$	$L^{salben}UO_2$	$L^{salben}UO_2K$	$L^{salben}UO_2Na$	$L^{salben}UO_2Ca$	$L^{salben}UO_2Y$
pK_a of $[M(H_2O)_m]^{n+}$	13.4	-	16.0	14.8	12.6	8.3
U–O7	-	1.783(8)	1.773(7)	1.782(5)	1.795(4)	1.771(6)
U–O8	-	1.792(7)	1.781(7)	1.780(5)	1.783(4)	1.788(7)
O1...O2	3.641	3.137	2.994	2.973	2.948	2.778
U...M	-	-	3.681(5)	3.668(3)	3.923(1)	3.884(1)
ω_{crown}^a	0.233	0.358	0.715	0.717	0.609	0.671
ω_{salben}^b	0.607	0.049	0.155	0.157	0.203	0.169
$\omega_{iminophenoxide}^c$	0.021, 0.055	0.012, 0.050	0.047, 0.129	0.043, 0.126	0.085, 0.083	0.076, 0.121

(a) Defined as root mean square deviation (rmsd) of the following atoms from the mean plane of their positions: O1, O2, O3, O4, O5, and O6. (b) RMSD of O1, O2, N1, N2, and N3. (c) RMSD of N1, O6, C1, C2, C3, C4, C5, C6 and C7; N2, O3, C14, C15, C16, C17, C18, C19 and C20. Atom labels are consistent with those given in the raw crystallographic data (see Supporting Information).

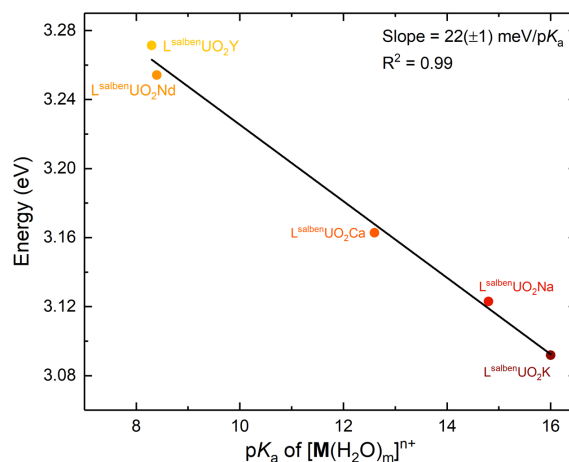
2.3 Electronic absorption spectroscopy

With these results in hand, we moved to interrogate the influence of redox-inactive metals on the electronic properties of the heterobimetallic complexes. The electronic absorption spectrum of the parent $L^{salben}UO_2$ complex displays three charge-transfer (CT) bands that appear to involve the UO_2^{2+} moiety, on the basis of their molar absorptivities ($\epsilon \approx 10^3 \text{ M}^{-1} \text{ cm}^{-1}$; see Figure 4). Two higher energy and higher absorptivity ($\epsilon \approx 10^4 \text{ M}^{-1} \text{ cm}^{-1}$) bands are also present at $\lambda < 350 \text{ nm}$; these are attributable to intraligand π -to- π^* transitions (see SI, Figure S16). Upon Lewis acid binding and formation of the heterobimetallic complexes, the π -to- π^* transitions undergo significant shifts (see SI, Figure S23), consistent with direct interaction between the Lewis acids and the macrocyclic ligand framework.

**Figure 4.** Stacked electronic absorption spectra of the $L^{salben}UO_2$ and $L^{salben}UO_2M$ complexes.

Closer examination of the energy of the CT bands for the heterobimetallic compounds with λ_{max} near 400 nm (Figure 4; deconvoluted with Gaussian fitting, see SI, Figure S18) as a function of the pK_a value of the incorporated Lewis acids reveals a linear trend with a slope of $22 \pm 1 \text{ meV}/pK_a$ (Figure 5). Thus, Lewis acids appear to reliably tune the electronic properties of UO_2^{2+} complexes, a phenomenon not previously explored. Trivalent redox-inactive cations engender the strongest

perturbations while mono- and divalent cations offer more modest shifts. Notably, the distinctive dependence of the absorption maximum near 400 nm for the $L^{salben}UO_2M$ complexes on pK_a is reminiscent of a similar relationship measured for our series of heterobimetallic complexes of nickel.²⁶ In those compounds, we found a corresponding slope of $46 \pm 5 \text{ meV}/pK_a$ for a similar CT band assigned in those cases as ligand-to-metal in character. Interestingly, the changes in the electronic absorption spectra as a function of Lewis acidity appear more modest (by a factor of ca. 2) for the case of UO_2^{2+} versus Ni.

**Figure 5.** Dependence of the lowest-energy absorption band (CT energy) of the $L^{salben}UO_2M$ complexes on the Lewis acidity (pK_a) of the corresponding M aqua complexes.

2.4 Electrochemistry

Having observed the apparent high stability of the heterobimetallic complexes in acetonitrile solutions, we were encouraged to investigate their electrochemical properties with cyclic voltammetry (CV) (Figure 6). Notably, electrochemical data has not been previously available for UO_2^{2+} held in close proximity to redox-inactive Lewis acids; this may be attributable to the poor stability of non-macrocyclic complexes of UO_2^{2+} containing other metals. To begin, CV data for $L^{salben}UO_2$ reveal a chemically reversible reduction at $E_{1/2} = -1.54 \text{ V}$ vs. ferrocenium/ferrocene (denoted hereafter as $Fc^{+/0}$; see SI and Figure S24 for

further details). The measured peak-to-peak separation, ΔE_p , of 76 mV at a scan rate of 100 mV/s is consistent with reasonably fast electron transfer. According to the criteria elaborated by Zanello and Connelly,³⁷ including the findings that the ratio of anodic and cathodic peak currents is near unity ($i_{p,a}/i_{p,c} \approx 1$), the value of $E_{1/2}$ is independent of scan rate, and ΔE_p is relatively near to the ideal 57 mV (see Figure S26), this process can be considered electrochemically reversible. Furthermore, on the basis of studies of similar non-macrocyclic monometallic UO_2^{2+} complexes, this process can be reliably assigned to $\text{U}^{\text{VI}}/\text{U}^{\text{V}}$ redox cycling.³⁸ As both the cathodic and anodic waves are linearly proportional to scan rate (see SI, Figure S25), both the U^{VI} and U^{V} forms of $\text{L}^{\text{salben}}\text{UO}_2$ are confirmed as freely diffusing.³⁹

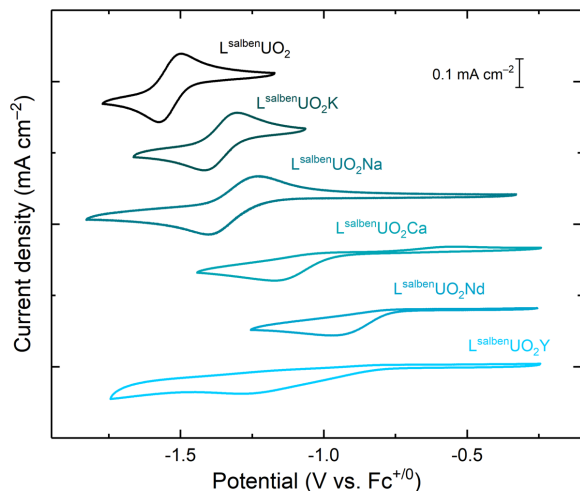


Figure 6. Cyclic voltammetry data for $\text{L}^{\text{salben}}\text{UO}_2$ and $\text{L}^{\text{salben}}\text{UO}_2\text{M}$ complexes (Conditions: 0.1 M $[\text{Bu}_4\text{N}]^+[\text{PF}_6]^-$ in CH_3CN ; scan rate: 100 mV/s; $[\text{U}] = 1 \text{ mM}$).

The potentials required for the reduction of $\text{L}^{\text{salben}}\text{UO}_2\text{K}$ and $\text{L}^{\text{salben}}\text{UO}_2\text{Na}$, -1.36 and -1.32 V vs. $\text{Fc}^{+/0}$ respectively, are consistent with retention of the coordinated Lewis acids resulting in shift of the $\text{U}^{\text{VI}}/\text{U}^{\text{V}}$ reduction potentials to more positive values. Scan rate-dependent studies reveal that both $\text{L}^{\text{salben}}\text{UO}_2\text{K}$ and $\text{L}^{\text{salben}}\text{UO}_2\text{Na}$ in both the U^{VI} and U^{V} states are freely diffusing (see SI, Figures S28 and S30). However, the measured ΔE_p values at 100 mV/s are greater at 89 mV and 181 mV, respectively, indicating diminished electrochemical reversibility and lower rates of electron transfer than that observed for $\text{L}^{\text{salben}}\text{UO}_2$.³⁷ Finally, we note that greater stability during redox cycling is encountered for $\text{L}^{\text{salben}}\text{UO}_2\text{K}$ than $\text{L}^{\text{salben}}\text{UO}_2\text{Na}$ (see SI, Figure S31). In particular, multiple cycling experiments (see SI, Figures S31 and S32) suggest that electrode fouling occurs upon reduction of $\text{L}^{\text{salben}}\text{UO}_2\text{Na}$, presumably attributable to chemical reactivity that follows the initial reduction; this theory is confirmed by experiments with polished or new electrodes (Figure S33). We anticipate the greater stability of the reduced form of $\text{L}^{\text{salben}}\text{UO}_2\text{K}$ is due to the better size match between 18-crown-6 moieties and K^+ (vs. Na^+).^{40,41}

The noted trends continue for $\text{L}^{\text{salben}}\text{UO}_2\text{Ca}$, which undergoes reduction with a peak cathodic potential ($E_{p,c}$) shifted to a more positive value of -1.18 V vs. $\text{Fc}^{+/0}$. The calcium complex behaves with yet poorer apparent electrochemical reversibility, displaying a quite large ΔE_p of 641 mV (see SI, Figure S34). CV data for $\text{L}^{\text{salben}}\text{UO}_2\text{Nd}$ reveal fully irreversible behavior, with only a single reduction observed with $E_{p,c} = -0.98$ V that is consistent with a freely diffusing compound retaining the coordinated Nd^{3+} ion (see SI, Figure S37). Finally, freely diffusing

$\text{L}^{\text{salben}}\text{UO}_2\text{Y}$ undergoes reduction at a more negative value of $E_{p,c} = -1.29$ V (see SI, Figure S39). The voltammetric response for this compound, however, is quite broad and thus consistent with markedly slowed electron transfer which complicates direct comparison of $E_{p,c}$ values with the other compounds in the series.

For the cases of $\text{L}^{\text{salben}}\text{UO}_2$ and $\text{L}^{\text{salben}}\text{UO}_2\text{K}$, one-electron reduction of the starting compounds to form $[\text{U}^{\text{V}}]$ species was confirmed through spectroelectrochemistry with UV-visible detection (see SI, Figures S44–S47 for data). Spectral changes in the range of 400 nm were observed upon reduction of both compounds, consistent with results from prior studies³⁸ showing generation of $[\text{U}^{\text{V}}]$ species. For $\text{L}^{\text{salben}}\text{UO}_2$, isosbestic points corresponding to generation of a single $[\text{U}^{\text{V}}]$ species were measured over 5 minutes at 357 and 413 nm. Similarly, spectra of $\text{L}^{\text{salben}}\text{UO}_2\text{K}$ revealed isosbestic points at 355 and 415 nm. However, a unique new feature was also observed at 650 nm upon reduction of $\text{L}^{\text{salben}}\text{UO}_2\text{K}$ suggesting influence of K^+ on the nascent $[\text{U}^{\text{V}}]$ product. Additional minor spectral changes were observed with $\text{L}^{\text{salben}}\text{UO}_2\text{K}$ over ca. 30 min, suggesting additional speciation occurs at longer times in this system. This is consistent with a role for the Lewis acid in promoting new reactivity, and thus future efforts will include efforts to isolate and characterize the products of (electro)chemical reduction of the heterobimetallic compounds described here.

Regarding general trends in the binding strengths of Lewis acidic metal ions M with the 18-crown-6-like cavity of L^{salben} , we find that the more Lewis acidic ion Y^{3+} can displace both K^+ and Ca^{2+} (see SI, Figures S41 and S42). Thus, although K^+ may be anticipated from supramolecular chemistry to have an ideal size match with the 18-crown-6 cavity, the greater Lewis acidity of Y^{3+} or Ca^{2+} (see SI, Figure S43) prevents K^+ from displacing these ions from the crown. However, NMR studies do confirm that K^+ displaces Na^+ in 1:1 competition experiments, in line with the better size match between 18-crown-6 and K^+ . This is also consistent with the similar Lewis acidities of K^+ and Na^+ ($pK_a = 16$ vs. 14.8, respectively).²⁷

3. DISCUSSION

In our previous work with heterobimetallic $[\text{Ni},\text{M}]$ complexes, we tabulated cathodic peak reduction potentials in order to quantify the influence of redox-inactive Lewis acids on $\text{Ni}^{\text{II}}/\text{Ni}^{\text{I}}$ reduction processes.²⁶ Taking the same strategy here for the $\text{L}^{\text{salben}}\text{UO}_2\text{M}$ series, plotting $E_{p,c}$ for the $\text{U}^{\text{VI}}/\text{U}^{\text{V}}$ reduction events versus the Lewis acid pK_a values reveals a slope of $61(\pm 9)$ mV/ pK_a (Figure 7). Data for Y^{3+} has been excluded from this analysis due to the obvious slow electron transfer encountered with $\text{L}^{\text{salben}}\text{UO}_2\text{Y}$, a phenomenon complicating understanding of the thermodynamic influence of Lewis acids on these systems. The trend for $E_{p,c}$ reveals that there is a clear and uniform trend of modulated reduction potential upon incorporation of Lewis acidic metals into macrocyclic UO_2^{2+} complexes. Similar to transition metal systems, trivalent Lewis acids result in the most pronounced shift in $E_{p,c}$.

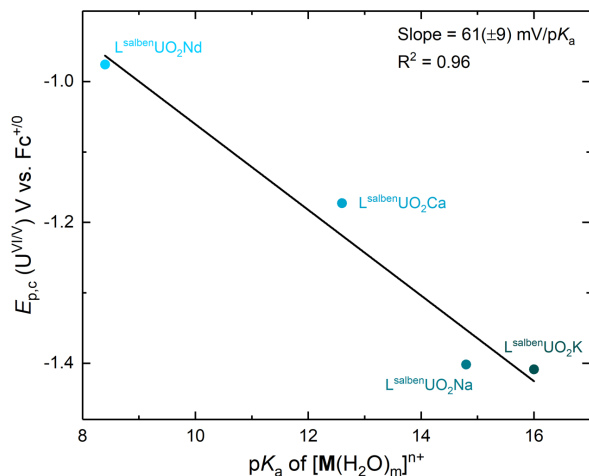


Figure 7. Plot of $E_{p,c}(U^{VI}/U^V)$ vs. pK_a of $[M(H_2O)_m]^{n+}$.

The shift of $E_{p,c}$ for the series of $L^{salben}UO_2M$ complexes is comparable to that measured for our prior $[Ni,M]$ complexes of $70(\pm 12)$ mV/ pK_a both in magnitude and estimated variance (15% vs. 17%, respectively). This suggests that the mechanism underlying tuning of actinyl ions' properties by Lewis acids may bear significant similarities to that operating with first-row transition metals. However, both our series of heterobimetallic compounds rely on phenolates that bridge between the redox-active U and Ni and the redox-inactive metals **M**. Thus, one contributor to the observed similar trends in redox behavior may be the common Lewis acid-driven tuning of the bridging ligands. On the other hand, *3d* and *5f* metals can be expected to experience different degrees of covalency in their coordination chemistry, suggesting that further investigation of these effects could be an appealing new strategy for study of metal-ligand covalency in the challenging *5f* elements. In any case, studies of these new effects could shed light on both the mechanism of Lewis acid tuning and changes that result in terms of structure and bonding (e.g., U–O bond order).

In addition to the uniform trend in $E_{p,c}$ observed for these heterobimetallic compounds, it is notable that the more Lewis acidic metals engender greater irreversibility to the reductive electrochemistry of the U^{VI}/U^V process. To investigate this phenomenon further, the heterogeneous electron-transfer rate constants were calculated for the heterobimetallic compounds that display both anodic and cathodic waves associated with the U^{VI}/U^V redox system, namely $L^{salben}UO_2K$, $L^{salben}UO_2Na$, and $L^{salben}UO_2Ca$. This was accomplished through the use of a standard working curve that allows conversion of the measured ΔE_p values to k^0 .^{42,43} Carrying out this calculation reveals that the k^0 values are 2.3, 0.7, and 0.029×10^{-3} cm s⁻¹, respectively. The wide span of values is intriguing, considering the compounds share the common supporting macrocyclic ligand L^{salben} . Even more intriguing, a plot of $\log k^0$ vs. pK_a of $[M(H_2O)_m]^{n+}$ reveals an essentially linear relationship (Figure 8). Consequently, we conclude that Lewis acidity governs not only the thermodynamics ($E_{1/2}$ value) of uranyl reduction in macrocyclic bimetallic complexes, but also strongly influences the kinetics (k^0) of uranyl reduction.

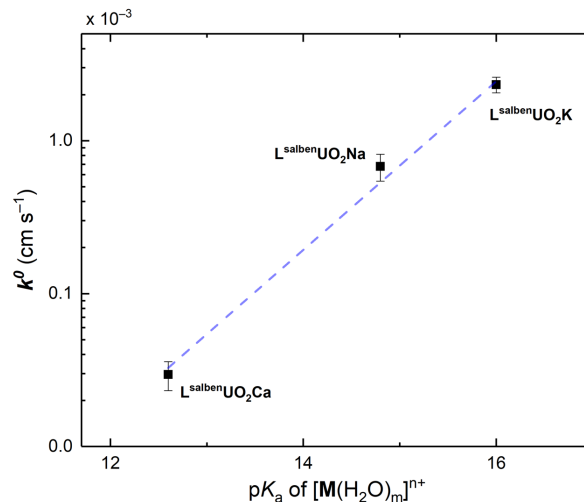


Figure 8. Plot of k^0 vs. pK_a of $[M(H_2O)_m]^{n+}$. R^2 for the linear fit is 0.99.

At this stage, we hypothesize that increasingly significant structural changes occur upon reduction of the adducts containing more Lewis acidic ions, resulting in greater reorganization upon reduction and thus the more irreversible behavior and attenuated values of k^0 . Considering minor oxidative waves appear at rather positive potentials for each of the $M = Ca^{2+}$, Nd^{3+} , Y^{3+} adducts following reduction (see SI, Figures S35, S37, and S39), these more robust Lewis acids appear to promote new chemical reactivity. As the subsequent re-oxidation features for Ca^{2+} , Nd^{3+} , and Y^{3+} adducts appear at similar potentials, the products of this new chemical reactivity may undergo dissociation of the redox-inactive metals to yield similar compounds. More generally, the data could imply that there is a common intermediate generated by the follow-up chemical reactivity. In any case, heterobimetallic complexes of UO_2^{2+} appear to offer a new platform for studying redox processes with this challenging ion, including reductive routes relevant to nuclear waste remediation. Chemical and electrochemical studies aimed at leveraging such a strategy are presently underway.

4. CONCLUSION

Redox-inactive Lewis acidic metals have been shown to be effective in uniformly tuning the electronic properties and reduction potential of the UO_2^{2+} ion in macrocyclic complexes. These findings have been enabled by synthesis of the first series of structurally characterized, macrocyclic, heterobimetallic actinide compounds. Similar to the case of model transition metal compounds, we find a shift in reduction potential of $61(\pm 9)$ mV/ pK_a for heterobimetallic compounds that feature redox-inactive metals that span a range in Lewis acidity from 16.0 (K^+) to 8.3 (Y^{3+}). Incorporation of the strongly Lewis acidic trivalent ion Nd^{3+} ($pK_a = 8.4$) results in a significant shift of $E_{p,c}(U^{VI}/U^V)$ to a potential that is 560 mV more positive than the corresponding monometallic precursor. These wide-ranging shifts differ from comparisons of electronic spectroscopic data, which indicate an attenuated influence of the Lewis acids in the case of the UO_2^{2+} compounds studied here. Electrochemical studies also suggest diminished electron transfer rates and thus implicate greater chemical reorganization upon reduction in systems featuring the more acidic di- and trivalent redox-inactive ions. Taken together, these findings reveal the scope of tuning possible with actinides by redox-inactive metals for the first time.

5. EXPERIMENTAL SECTION

5.1 General Considerations

All manipulations were carried out in dry N₂-filled gloveboxes (Vacuum Atmospheres Co., Hawthorne, CA) or under N₂ atmosphere using standard Schlenk techniques unless otherwise noted. All solvents were of commercial grade and dried over activated alumina using a PPT Glass Contour (Nashua, NH) solvent purification system prior to use, and were stored over molecular sieves. All chemicals were from major commercial suppliers and used as received or after extensive drying. 2,3-dihydroxybenzaldehyde was sublimed in vacuo before use. CD₃CN was purchased from Cambridge Isotope Laboratories and dried over 3 Å molecular sieves. ¹H, ¹³C, and ¹⁹F NMR spectra were collected on 400 and 500 MHz Bruker spectrometers and referenced to the residual protio-solvent signal⁴⁴ in the case of ¹H and ¹³C. ¹⁹F NMR spectra were referenced and reported relative to CCl₃F as an external standard following the recommended scale based on ratios of absolute frequencies ($\bar{\nu}$).^{45,46} Chemical shifts (δ) are reported in units of ppm and coupling constants (J) are reported in Hz. NMR spectra are given in the SI (Figures S1 to S15). Electronic absorption spectra were collected with an Ocean Optics Flame spectrometer, in a 1-cm path length quartz cuvette.

Regarding special safety precautions needed for this work, depleted uranium is a weak alpha-particle emitter; all manipulations of U-containing materials should be carried out in a laboratory equipped with appropriate radiation safety protocols.

5.2 Electrochemical Methods

Electrochemical experiments were carried out in a N₂-filled glovebox in dry, degassed CH₃CN. 0.10 M tetra(n-butylammonium) hexafluorophosphate ([ⁿBu₄N]⁺[PF₆]⁻; Sigma-Aldrich, electrochemical grade) served as the supporting electrolyte. Measurements were made with a Gamry Reference 600+ Potentiostat/Galvanostat using a standard three-electrode configuration. The working electrode was the basal plane of highly oriented pyrolytic graphite (HOPG) (GraphiteStore.com, Buffalo Grove, Ill.; surface area: 0.09 cm²), the counter electrode was a platinum wire (Kurt J. Lesker, Jefferson Hills, PA; 99.99%, 0.5 mm diameter), and a silver wire immersed in electrolyte served as a pseudoreference electrode (CH Instruments). The reference was separated from the working solution by a Vycor frit (Bioanalytical Systems, Inc.). Ferrocene (Sigma Aldrich; twice-sublimed) was added to the electrolyte solution prior to the beginning of each experiment; the midpoint potential of the ferrocenium/ferrocene couple (denoted as Fc⁺⁰) served as an external standard for comparison of the recorded potentials. The average peak-to-peak potential (ΔE_p) for Fc⁺⁰ across the experiments reported in this paper was 91(±19) mV. Concentrations of analyte for cyclic voltammetry were ca. 0.1 to 1 mM unless otherwise noted.

Spectroelectrochemistry was carried out in the same glovebox as described above (N₂ atmosphere), with 0.10 M [ⁿBu₄N]⁺[PF₆]⁻ in CH₃CN electrolyte for L^{salben}UO₂K and 0.10 M [ⁿBu₄N]⁺[PF₆]⁻ in DMF electrolyte for L^{salben}UO₂. A thin layer quartz cell was used with a Teflon cap for housing the electrodes (ALS Co., Ltd., path length: 1.0 mm). The working electrode was a platinum mesh/flag electrode covered with a PTFE shrink tube up to the flag, and the counter and reference electrodes were both platinum wires (ALS Co., Ltd.).

5.3 Synthesis and characterization

Synthesis of 3,3'-(3,6-Dioxaoctane-1,8-diylidioxy)bis(2-hydroxybenzaldehyde). Under an inert atmosphere of nitrogen, a dry Schlenk flask was loaded with 2,3-dihydroxybenzaldehyde (3.0 g, 21.7 mmol) dissolved in 10 mL of dry THF. This solution was transferred using a syringe to a suspension of NaH (1.15 g, 47.8 mmol) in 10 mL of dry THF under N₂ over a period of 2 hours. The temperature was kept below 25°C. The color change to bright yellow indicates the formation of disodium salt of 2,3-dihydroxybenzaldehyde. The ice bath was removed after addition and the mixture was stirred for 1 hour at room temperature. Under a positive flow of N₂, triethylene glycol ditosylate (5.0 g, 10.9 mmol) dissolved in 30 mL of dry THF was added to the yellow mixture in a single aliquot using a syringe. The resulting mixture was then stirred for 60 hours under static N₂ atmosphere. Addition of 100 mL of water resulted in a dark brown solution that was extracted twice with CHCl₃. The aqueous layer was treated with 6 M HCl until the pH of the mixture was 1. This mixture was then extracted with three portions of CHCl₃. The combined organic layers were washed with 1 M HCl and dried over anhydrous MgSO₄. Evaporation of solvent yielded a pale-yellow solid which was used without any further purification. Yield: 93% (4.0 g). Spectroscopic characterization by ¹H NMR (see SI, Figure S1) confirms the expected structure in agreement with a prior literature report.³²

Synthesis of L^{salben}H₂Ba. To a three-necked flask, Ba(OTf)₂ (4.46 g, 10.2 mmol) dissolved in 1 L of CH₃OH (0.01 M) and 1 equiv. of 3,3'-(3,6-Dioxaoctane-1,8-diylidioxy)bis(2-hydroxybenzaldehyde) (4.0 g, 10.2 mmol) in 100 mL THF (0.1 M) were added slowly under reflux. 1 equiv. of N-Methyl-2,2'-diaminodiethylamine (1.2 g, 10.2 mmol) in 100 mL CH₃OH (0.1 M) was added dropwise over a period of 6 hours. The reaction mixture was refluxed for 30 minutes. After cooling down to room temperature the resulting yellow colored solution was evaporated on the rotary evaporator and Schlenk line and washed with diethyl ether to give yellow crystalline solid. Crystals suitable for X-ray diffraction were obtained by vapor diffusion of diethyl ether into a solution of L^{salben}H₂Ba in CH₃CN.

L^{salben}H₂Ba. Yield: 95%. ¹H NMR (400 MHz, CD₃CN) δ (ppm): 13.60 (bs, 2H), 8.30 (s, 1H), 8.27 (s, 1H), 6.96 – 6.89 (m, 4H), 6.46 (t, ³J_{H,H} = 7.9 Hz), 4.20 – 4.16 (m, 4H), 3.98 – 4.02 (m, 4H), 3.84 (s, 4H), 3.69 – 3.63 (m, 4H), 2.78 – 2.73 (m, 4H), 2.37 (s, 3H). ¹⁹F NMR (376 Hz, CD₃CN) δ –80.12. ¹³C{¹H} NMR (126 MHz, CD₃CN) δ (ppm): 168.34, 151.96, 127.02, 123.16, 120.61, 116.12, 114.64, 113.65, 70.95, 70.13, 67.53, 59.09, 51.21, 44.56.

Elemental analysis for L^{salben}H₂Ba was performed by Midwest Micro-lab, Inc. (Indianapolis, IN). Anal. Calcd. for C₂₇H₃₃N₃O₁₂F₆S₂Ba (L^{salben}H₂Ba): C 35.75, H 3.67, N 4.63; Found: C 35.81, H 3.74, N 4.39.

Synthesis of L^{salben}UO₂. An excess of guanidinium sulfate (1.76 g, 8.16 mmol) dissolved in water was added to a suspension of L^{salben}Ba (370 mg, 0.41 mmol) in CHCl₃ under stirring until the organic layer was clear. The organic layer was separated, concentrated and diluted using MeOH. To this yellow solution, 1 equiv. of UO₂(OAc)₂·2H₂O dissolved in MeOH was added and the mixture was stirred for overnight. The resulting red precipitate was filtered and washed with cold MeOH. Crystals suitable for X-ray diffraction were obtained by vapor diffusion of diethyl ether into a DMF solution of L^{salben}UO₂. Spectroscopic char-

acterization by ^1H NMR confirmed the expected structure in agreement with a prior literature report.³⁵

$\text{L}^{\text{salben}}\text{UO}_2$. Yield: 50%. ^1H NMR (500 MHz, CD_3CN) δ (ppm): 9.56 (s, 2H), 7.30 (d, $^3J_{\text{H,H}} = 7.8$ Hz, 2H), 7.24 (d, $^3J_{\text{H,H}} = 7.8$ Hz, 2H), 6.71 (t, $^3J_{\text{H,H}} = 7.9$ Hz, 2H), 5.02 (t, $^3J_{\text{H,H}} = 14.0$ Hz, 2H), 4.62 – 4.58 (m, 2H), 4.41 (t, $^3J_{\text{H,H}} = 4.1$ Hz, 4H), 4.11 – 3.97 (m, 4H), 3.95 – 3.87 (m, 2H), 3.84 (s, 4H), 3.65 – 3.57 (m, 2H), 3.22 (s, 3H). Anal. Calcd. for $\text{C}_{25}\text{H}_{31}\text{N}_3\text{O}_8\text{U}$ ($\text{L}^{\text{salben}}\text{UO}_2$): C 40.60, H 4.23, N 5.68; Found: C 35.17, H 3.32, N 3.81. Cyclic Voltammetry (0.1 M $[\text{Bu}_4\text{N}]^+[\text{PF}_6]^-$ in CH_3CN): $E_{1/2} = -1.54$ V vs. $\text{Fc}^{+/0}$. Electronic absorption spectrum in CH_3CN ($\text{M}^{-1}\text{cm}^{-1}$): 243 (11500), 272 (7300), 337 (3000), 402 (1800), 482 (514) nm.

Synthesis of $\text{L}^{\text{salben}}\text{UO}_2\text{M}$ complexes. Under an inert atmosphere, a heterogeneous solution of $\text{L}^{\text{salben}}\text{UO}_2$ in CH_3CN was added to 1 equiv. of corresponding metal salt solution in CH_3CN and stirred overnight. The color change depends on the identity of the metal triflate salt used; the product color ranges from pale red to orange to yellow as a function of increasing Lewis acidity. The solvent was removed in vacuo to give the desired product. Yields were typically in the range of 85-95%. Crystals suitable for X-ray diffraction were obtained by vapor diffusion of diethyl ether into a CH_3CN solution of the $\text{L}^{\text{salben}}\text{UO}_2\text{M}$ complexes for $\text{L}^{\text{salben}}\text{UO}_2\text{K}$, $\text{L}^{\text{salben}}\text{UO}_2\text{Na}$, and $\text{L}^{\text{salben}}\text{UO}_2\text{Y}$. Crystals of $\text{L}^{\text{salben}}\text{UO}_2\text{Ca}$ suitable for X-ray diffraction were obtained by vapor diffusion of diethyl ether into a CH_3OH solution stored outside the glovebox.

Elemental analyses for $\text{L}^{\text{salben}}\text{UO}_2$ and the $\text{L}^{\text{salben}}\text{UO}_2\text{M}$ complexes were performed by the UC Berkeley Microanalytical Facility (Berkeley, CA). Due to limitations in sample handling procedures for these acutely moisture-sensitive compounds, satisfactory analysis ($\pm 0.4\%$) could not be obtained for four of the five new heterobimetallic compounds reported here and $\text{L}^{\text{salben}}\text{UO}_2$. Satisfactory analysis was obtained for $\text{L}^{\text{salben}}\text{UO}_2\text{Nd}$.

$\text{L}^{\text{salben}}\text{UO}_2\text{K}$. Yield: 94%. ^1H NMR (500 MHz, CD_3CN) δ (ppm): 9.60 (s, 2H), 7.54 (d, $^3J_{\text{H,H}} = 8.0$ Hz, 2H), 7.49 (d, $^3J_{\text{H,H}} = 8.0$ Hz, 2H), 7.11 (t, $^3J_{\text{H,H}} = 8.0$ Hz, 2H), 5.17 – 5.07 (m, 2H), 4.86 – 4.74 (m, 6H), 4.42 (t, $^3J_{\text{H,H}} = 4.5$ Hz, 4H), 4.35 (s, 4H), 4.10 – 4.01 (m, 2H), 3.96 – 3.86 (m, 2H), 3.40 (s, 3H). ^{19}F NMR (376 Hz, CD_3CN) δ -79.28. Anal. Calcd. for $\text{C}_{26}\text{H}_{31}\text{F}_3\text{KN}_3\text{O}_{11}\text{SU}$ ($\text{L}^{\text{salben}}\text{UO}_2\text{K}$): C 33.66, H 3.37, N 4.53; Found: C 29.02, H 3.60, N 2.97. Cyclic Voltammetry (0.1 M $[\text{Bu}_4\text{N}]^+[\text{PF}_6]^-$ in CH_3CN): $E_{1/2} = -1.36$ V vs. $\text{Fc}^{+/0}$. Electronic absorption spectrum in CH_3CN ($\text{M}^{-1}\text{cm}^{-1}$): 246 (13900), 272 (12100), 329 (6200), 401 (1800), 478 (1200) nm.

$\text{L}^{\text{salben}}\text{UO}_2\text{Na}$. Yield: 89%. ^1H NMR (500 MHz, CD_3CN) δ (ppm): 9.53 (s, 2H), 7.40 (d, $^3J_{\text{H,H}} = 7.8$ Hz, 2H), 7.30 (d, $^3J_{\text{H,H}} = 7.8$ Hz, 2H), 6.95 (t, $^3J_{\text{H,H}} = 7.8$ Hz, 2H), 5.10 – 5.00 (m, 2H), 4.66 – 4.58 (m, 2H), 4.43 – 4.38 (m, 4H), 3.95 – 3.91 (m, 4H), 3.84 – 3.80 (m, 6H), 3.72 – 3.69 (m, 2H), 3.27 (s, 3H). ^{19}F NMR (376 Hz, CD_3CN) δ -80.19. Anal. Calcd. for $\text{C}_{26}\text{H}_{31}\text{F}_3\text{NaN}_3\text{O}_{11}\text{SU}$ ($\text{L}^{\text{salben}}\text{UO}_2\text{Na}$): C 34.26, H 3.43, N 4.61; Found: C 35.95, H 3.54, N 4.74. Cyclic Voltammetry (0.1 M $[\text{Bu}_4\text{N}]^+[\text{PF}_6]^-$ in CH_3CN): $E_{1/2} = -1.32$ V vs. $\text{Fc}^{+/0}$. Electronic absorption spectrum in CH_3CN ($\text{M}^{-1}\text{cm}^{-1}$): 247 (12700), 272 (13100), 329 (6900), 397 (3500), 483 (1000) nm.

$\text{L}^{\text{salben}}\text{UO}_2\text{Ca}$. Yield: 90%. ^1H NMR (500 MHz, CD_3CN) δ (ppm): 9.56 (s, 2H), 7.47 (d, $^3J_{\text{H,H}} = 7.8$ Hz, 2H), 7.40 (d, $^3J_{\text{H,H}} = 7.8$ Hz, 2H), 6.81 (t, $^3J_{\text{H,H}} = 7.8$ Hz, 2H), 5.13 – 5.04 (m, 2H), 4.75 – 4.66 (m, 2H), 4.53 (t, $^3J_{\text{H,H}} = 4.4$ Hz, 4H), 4.12 (t, $^3J_{\text{H,H}} = 4.4$ Hz, 4H), 4.03 – 3.95 (m, 6H), 3.82 – 3.76 (m, 2H), 3.33 (s, 3H). ^{19}F NMR (376 Hz, CD_3CN) δ

-80.16. Anal. Calcd. for $\text{C}_{27}\text{H}_{31}\text{CaF}_6\text{N}_3\text{O}_{14}\text{S}_2\text{U}$ ($\text{L}^{\text{salben}}\text{UO}_2\text{Ca}$): C 30.09, H 2.90, N 3.90; Found: C 26.81, H 2.09, N 2.36. Cyclic Voltammetry (0.1 M $[\text{Bu}_4\text{N}]^+[\text{PF}_6]^-$ in CH_3CN): $E_{\text{p,c}} = -1.17$ V vs. $\text{Fc}^{+/0}$. Electronic absorption spectrum in CH_3CN ($\text{M}^{-1}\text{cm}^{-1}$): 243 (13300), 272 (12800), 314 (8400), 392 (3300), 473 (900) nm.

$\text{L}^{\text{salben}}\text{UO}_2\text{Y}$. Yield: 87%. ^1H NMR (500 MHz, CD_3CN) δ (ppm): 9.56 (t, 2H), 7.38 – 7.34 (dd, $^3J_{\text{H,H}} = 8.0$ Hz, $^4J_{\text{H,H}} = 1.3$ Hz, 2H), 7.28 – 7.24 (dd, $^3J_{\text{H,H}} = 8.0$ Hz, $^4J_{\text{H,H}} = 1.3$ Hz, 2H), 6.78 (t, $^3J_{\text{H,H}} = 7.9$ Hz, 2H), 5.06 – 4.98 (m, 2H), 4.64 – 4.57 (m, 2H), 4.40 – 4.32 (m, 4H), 3.98 (t, $^3J_{\text{H,H}} = 4.3$ Hz, 4H), 3.92 – 3.85 (m, 2H), 3.84 (s, 4H), 3.69 – 3.64 (m, 2H), 3.22 (s, 3H). ^{19}F NMR (376 Hz, CD_3CN) δ -79.40. Anal. Calcd. for $\text{C}_{30}\text{H}_{34}\text{F}_9\text{N}_4\text{O}_{17}\text{S}_3\text{UY}$ ($\text{L}^{\text{salben}}\text{UO}_2\text{Y} + \text{CH}_3\text{CN}$): C 27.37, H 2.60, N 4.26; Found: C 24.89, H 2.07, N 2.88. Cyclic Voltammetry (0.1 M $[\text{Bu}_4\text{N}]^+[\text{PF}_6]^-$ in CH_3CN): $E_{\text{p,c}} = -1.29$ V vs. $\text{Fc}^{+/0}$. Electronic absorption spectrum in CH_3CN ($\text{M}^{-1}\text{cm}^{-1}$): 240 (11500), 272 (12100), 322 (6700), 379 (3100), 470 (600) nm.

$\text{L}^{\text{salben}}\text{UO}_2\text{Nd}$. Yield: 91%. ^1H NMR (500 MHz, CD_3CN) δ (ppm): 11.01, 10.29, 9.39, 8.30, 7.86, 5.87, 5.55, 4.74, 4.45, 3.95, 3.42, 2.45. ^{19}F NMR (376 Hz, CD_3CN) δ -79.80. Anal. Calcd. for $\text{C}_{28}\text{H}_{31}\text{F}_9\text{N}_3\text{NdO}_{17}\text{S}_3\text{U}$ ($\text{L}^{\text{salben}}\text{UO}_2\text{Nd}$): C 25.27, H 2.35, N 3.16; Found: C 25.17, H 2.21, N 3.05. Cyclic Voltammetry (0.1 M $[\text{Bu}_4\text{N}]^+[\text{PF}_6]^-$ in CH_3CN): $E_{\text{p,c}} = -0.98$ V vs. $\text{Fc}^{+/0}$. Electronic absorption spectrum in CH_3CN ($\text{M}^{-1}\text{cm}^{-1}$): 242 (11700), 272 (12400), 322 (7200), 381 (3300), 477 (600) nm.

5.4 X-ray crystallographic data

CCDC entries 1960625, 1960626, and 1960628–1960631 contain the supplementary crystallographic data for this paper. These data can be obtained free of charge from the Cambridge Crystallographic Data Centre. For details regarding collection and refining of the data see the Supporting Information.

ASSOCIATED CONTENT

Supporting Information

Supporting Information is available free of charge on the ACS Publications website: Experimental details; synthesis and characterization of compounds used in this study; NMR spectra; crystallographic details; electronic absorption spectra; electrochemical data (PDF); Cartesian coordinates (XYZ) from single-crystal XRD studies.

AUTHOR INFORMATION

Corresponding Author

* To whom correspondence should be addressed. E-mail: blake-more@ku.edu, phone: +1 (785) 864-3019 (J.D.B.)

Present Addresses

† Department of Chemistry, Franklin & Marshall College, P.O. Box 3003, Lancaster, Pennsylvania 17604, United States

Author Contributions

The manuscript was written through contributions of all authors. All authors have given approval to the final version of the manuscript.

Notes

The authors declare no competing financial interests.

ACKNOWLEDGMENT

The authors thank Dr. Justin Douglas and Sarah Neuenswander for assistance with NMR spectroscopy, and Michael Lemon and Alice Dale for assistance with radiation safety protocols. This work was supported by the US Department of Energy, Office of Science, Office of Basic Energy Sciences through the Early Career Research Program (DE-SC0019169). The authors also acknowledge the US National Institutes of Health for support of the NMR instrumentation (S10OD016360 and S10RR024664) used in this study.

REFERENCES

- (1) Marçalo, J.; Gibson, J. K. Gas-Phase Energetics of Actinide Oxides: An Assessment of Neutral and Cationic Monoxides and Dioxides from Thorium to Curium. *J. Phys. Chem. A* **2009**, *113*, 12599-12606.
- (2) Neidig, M. L.; Clark, D. L.; Martin, R. L. Covalency in f-element complexes. *Coord. Chem. Rev.* **2013**, *257*, 394-406.
- (3) Kaltsoyannis, N.; Scott, P. *The f elements*. Oxford University Press Inc.: New York, 1999; p. 36.
- (4) Meinrath, G. Coordination of uranyl(VI) carbonate species in aqueous solutions. *J. Radioanal and Nuclear Chem.* **1996**, *211*, 349-362.
- (5) Cowie, B. E.; Purkis, J. M.; Austin, J.; Love, J. B.; Arnold, P. L. Thermal and Photochemical Reduction and Functionalization Chemistry of the Uranyl Dication, $[U^{VI}O_2]^{2+}$. *Chem. Rev.* **2019**, *119*, 10595-10637.
- (6) Arnold, P. L.; Patel, D.; Wilson, C.; Love, J. B. Reduction and selective oxo group silylation of the uranyl dication. *Nature* **2008**, *451*, 315.
- (7) Schnaars, D. D.; Wu, G.; Hayton, T. W. Silylation of the Uranyl Ion Using $B(C_6F_5)_3$ -Activated Et_3SiH . *Inorg. Chem.* **2011**, *50*, 9642-9649.
- (8) Bell, N. L.; Shaw, B.; Arnold, P. L.; Love, J. B. Uranyl to Uranium(IV) Conversion through Manipulation of Axial and Equatorial Ligands. *J. Am. Chem. Soc.* **2018**, *140*, 3378-3384.
- (9) Arnold, P. L.; Pécharman, A.-F.; Hollis, E.; Yahia, A.; Maron, L.; Parsons, S.; Love, J. B. Uranyl oxo activation and functionalization by metal cation coordination. *Nat. Chem.* **2010**, *2*, 1056.
- (10) Zegke, M.; Nichol, G. S.; Arnold, P. L.; Love, J. B. Catalytic one-electron reduction of uranyl(VI) to Group 1 uranyl(V) complexes via Al(III) coordination. *Chem. Commun.* **2015**, *51*, 5876-5879.
- (11) Faizova, R.; White, S.; Scopelliti, R.; Mazzanti, M. The effect of iron binding on uranyl(V) stability. *Chem. Sci.* **2018**, *9*, 7520-7527.
- (12) McEvoy, J. P.; Brudvig, G. W. Water-Splitting Chemistry of Photosystem II. *Chem. Rev.* **2006**, *106*, 4455-4483.
- (13) Yano, J.; Yachandra, V. Mn_4Ca Cluster in Photosynthesis: Where and How Water is Oxidized to Dioxygen. *Chem. Rev.* **2014**, *114*, 4175-4205.
- (14) Kanady, J. S.; Tsui, E. Y.; Day, M. W.; Agapie, T. A Synthetic Model of the Mn_3Ca Subsite of the Oxygen-Evolving Complex in Photosystem II. *Science* **2011**, *333*, 733-736.
- (15) Tsui, E. Y.; Tran, R.; Yano, J.; Agapie, T. Redox-inactive metals modulate the reduction potential in heterometallic manganese-oxido clusters. *Nat. Chem.* **2013**, *5*, 293.
- (16) Yiu, S.-M.; Man, W.-L.; Lau, T.-C. Efficient Catalytic Oxidation of Alkanes by Lewis Acid/ $[Os^{VI}(N)Cl_4]^-$ Using Peroxides as Terminal Oxidants. Evidence for a Metal-Based Active Intermediate. *J. Am. Chem. Soc.* **2008**, *130*, 10821-10827.
- (17) Du, H.; Lo, P.-K.; Hu, Z.; Liang, H.; Lau, K.-C.; Wang, Y.-N.; Lam, W. W. Y.; Lau, T.-C. Lewis acid-activated oxidation of alcohols by permanganate. *Chem. Commun.* **2011**, *47*, 7143-7145.
- (18) Fukuzumi, S.; Morimoto, Y.; Kotani, H.; Naumov, P.; Lee, Y.-M.; Nam, W. Crystal structure of a metal ion-bound oxoiron(IV) complex and implications for biological electron transfer. *Nat. Chem.* **2010**, *2*, 756.
- (19) Bang, S.; Lee, Y.-M.; Hong, S.; Cho, K.-B.; Nishida, Y.; Seo, M. S.; Sarangi, R.; Fukuzumi, S.; Nam, W. Redox-inactive metal ions modulate the reactivity and oxygen release of mononuclear non-haem iron(III)-peroxo complexes. *Nat. Chem.* **2014**, *6*, 934.
- (20) Park, Y. J.; Ziller, J. W.; Borovik, A. S. The Effects of Redox-Inactive Metal Ions on the Activation of Dioxygen: Isolation and Characterization of a Heterobimetallic Complex Containing a $Mn^{III}-(\mu-OH)-Ca^{II}$ Core. *J. Am. Chem. Soc.* **2011**, *133*, 9258-61.
- (21) Lacy, D. C.; Park, Y. J.; Ziller, J. W.; Yano, J.; Borovik, A. S. Assembly and Properties of Heterobimetallic Co^{III}/Ca^{II} Complexes with Aquo and Hydroxo Ligands. *J. Am. Chem. Soc.* **2012**, *134*, 17526-35.
- (22) Horwitz, C. P.; Ciringh, Y. Synthesis and electrochemical properties of oxo-bridged manganese dimers incorporating alkali and alkaline-earth cations. *Inorg. Chim. Acta* **1994**, *225*, 191-200.
- (23) Reath, A. H.; Ziller, J. W.; Tsay, C.; Ryan, A. J.; Yang, J. Y. Redox Potential and Electronic Structure Effects of Proximal Nonredox Active Cations in Cobalt Schiff Base Complexes. *Inorg. Chem.* **2017**, *56*, 3713-3718.
- (24) Chantarojsiri, T.; Ziller, J. W.; Yang, J. Y. Incorporation of redox-inactive cations promotes iron catalyzed aerobic C-H oxidation at mild potentials. *Chem. Sci.* **2018**, *9*, 2567-2574.
- (25) Matsunaga, S.; Shibasaki, M., Multimetallic Schiff base complexes as cooperative asymmetric catalysts. *Synthesis* **2013**, *45*, 421-437.
- (26) Kumar, A.; Lionetti, D.; Day, V. W.; Blakemore, J. D. Trivalent Lewis Acidic Cations Govern the Electronic Properties and Stability of Heterobimetallic Complexes of Nickel. *Chem. Eur. J.* **2018**, *24*, 141-149.
- (27) Perrin, D. D. *Ionisation Constants of Inorganic Acids and Bases in Aqueous Solution*. Pergamon, 1982.
- (28) Solari, E.; Corazza, F.; Floriani, C.; Chiesi-Villa, A.; Guastini, C., Polydentate ligand exchange via formation of a dimetallic complex. Crystal structures of $[(thf)Fe(acen)MCl_2]$ ($M = Fe$ or Zn), $[ClFe(salphen)FeCl(thf)_2]$, $[Ti(acen)(thf)_2][CoCl_3(thf)]$, and $[Ti(acen)(thf)_2][Fe_3Cl_8(thf)_2][acen=N,N'$ -ethylenebis(acetylacetonimine), $salphen=N,N'$ -ophenylenebis(salicylideneimine), and $thf =$ tetrahydrofuran]. *J. Chem. Soc., Dalton Trans.* **1990**, 1345-1355.
- (29) Guerriero, P.; Tamburini, S.; Vigato, P. A.; Russo, U.; Benelli, C., Mössbauer and magnetic properties of mononuclear, homo- and heterodinuclear complexes. *Inorg. Chim. Acta* **1993**, *213*, 279-287.
- (30) Matsunaga, S.; Shibasaki, M., Recent advances in cooperative bimetallic asymmetric catalysis: dinuclear Schiff base complexes. *Chem. Commun.* **2014**, *50*, 1044-1057.
- (31) Van Staveren, C. J.; Fenton, D. E.; Reinhoudt, D. N.; Van Eerden, J.; Harkema, S. Co-complexation of urea and UO_2^{2+} in a Schiff base macrocycle: a mimic of an enzyme binding site. *J. Am. Chem. Soc.* **1987**, *109*, 3456-3458.
- (32) Van Staveren, C. J.; Van Eerden, J.; Van Veggel, F. C. J. M.; Harkema, S.; Reinhoudt, D. N. Cocomplexation of neutral guests and electrophilic metal cations in synthetic macrocyclic hosts. *J. Am. Chem. Soc.* **1988**, *110*, 4994-5008.
- (33) Zanello, P.; Cinquantini, A.; Guerriero, P.; Tamburini, S.; Vigato, P. A. Electrochemical behaviour of acyclic and macrocyclic complexes of nickel(II), copper(II) and uranyl(VI). *Inorg. Chim. Acta* **1986**, *117*, 91-96.
- (34) Casellato, U.; Tamburini, S.; Tomasin, P.; Vigato, P. A.; Aime, S.; Botta, M. Synthesis, X-ray Structure, and Solution NMR Studies of Ln(III) Complexes with a Macrocyclic Asymmetric Compartmental Schiff Base. Preference of the Ln(III) Ions for a Crown-Like Coordination Site. *Inorg. Chem.* **1999**, *38*, 2906-2916.
- (35) Brianese, N.; Casellato, U.; Tamburini, S.; Tomasin, P.; Vigato, P. A., Asymmetric compartmental macrocyclic ligands and related mononuclear and hetero-dinuclear complexes with d- and/or f-metal ions. *Inorg. Chim. Acta* **1999**, *293*, 178-194.

- (36) Casellato, U.; Tamburini, S.; Tomasin, P.; Vigato, P. A. Uranyl(VI) complexes with [1+1] asymmetric compartmental ligands containing a Schiff base and a crown ether-like chamber. *Inorg. Chim. Acta* **2002**, *341*, 118-126
- (37) Zanello, P.; Connelly, N. G., *Inorganic Electrochemistry: Theory, Practice and Application*. Royal Society of Chemistry: Cambridge, 2003, pp. 55-58.
- (38) Mizuoka, K.; Kim, S.-Y.; Hasegawa, M.; Hoshi, T.; Uchiyama, G.; Ikeda, Y. Electrochemical and Spectroelectrochemical Studies on $\text{UO}_2(\text{saloph})\text{L}$ (saloph = *N,N'*-Disalicylidene-*o*-phenylenediaminate, L = Dimethyl Sulfoxide or *N,N'*-Dimethylformamide). *Inorg. Chem.* **2003**, *42*, 1031-1038.
- (39) Savéant, J.-M., *Elements of Molecular and Biomolecular Electrochemistry*. Wiley: Hoboken, NJ, 2006.
- (40) Pedersen, C. J. Cyclic polyethers and their complexes with metal salts. *J. Am. Chem. Soc.* **1967**, *89*, 7017-7036.
- (41) Blakemore, J. D.; Chitta, R.; D'Souza, F. Synthesis and study of crown ether-appended boron dipyrin chemosensors for cation detection. *Tet. Lett.* **2007**, *48*, 1977-1982.
- (42) Nicholson, R. S., Theory and application of cyclic voltammetry for measurement of electrode reaction kinetics. *Anal. Chem.* **1965**, *37*, 1351-1355.
- (43) Bard, A. J.; Faulkner, L. R., *Electrochemical Methods: Fundamentals and Applications*. 2nd ed.; Wiley: Hoboken, NJ, 2001.
- (44) Fulmer, G. R.; Miller, A. J. M.; Sherden, N. H.; Gottlieb, H. E.; Nudelman, A.; Stoltz, B. M.; Bercaw, J. E.; Goldberg, K. I. NMR Chemical Shifts of Trace Impurities: Common Laboratory Solvents, Organics, and Gases in Deuterated Solvents Relevant to the Organometallic Chemist. *Organometallics* **2010**, *29*, 2176-2179.
- (45) Harris, R.K.; Becker, E.D.; Cabral de Menezes, S.M.; Goodfellow, R.; Granger, P. NMR nomenclature. Nuclear spin properties and conventions for chemical shifts (IUPAC Recommendations 2001). *Pure Appl. Chem.* **2001**, *73*, 1795-1818.
- (46) Harris, R.K.; Becker, E.D.; Cabral de Menezes, S.M.; Granger, P.; Hoffman, R.E.; Zilm, K.W. Further conventions for NMR shielding and chemical shifts (IUPAC Recommendations 2008). *Pure Appl. Chem.* **2008**, *80*, 59-84.

TOC Graphic

